

## High Range Resolution Radar Measurements of the Speed Distribution of Breaking Events in Wind-Generated Ocean Waves: Surface Impulse and Wave Energy Dissipation Rates

O. M. PHILLIPS

*Department of Earth and Planetary Sciences, The Johns Hopkins University, Baltimore, Maryland*

F. L. POSNER AND J. P. HANSEN

*Radar Division, Naval Research Laboratory, Washington, D.C.*

(Manuscript received 8 December 1999, in final form 3 April 2000)

### ABSTRACT

A set of X-band radar measurements, backscattered from the sea surface at near grazing incidence with very high spatial and temporal resolution (30 cm in range and 2000-Hz pulse repetition frequency) in moderate wind conditions, are dominated by moving discrete events (sea spikes). They have radar cross sections of up to about  $1 \text{ m}^2$  and are found to possess the characteristics of breaking wave fronts. Contributions from Bragg backscattering appear to be at least two orders of magnitude smaller. The number of events detected per unit area per unit time was of the same order as found by Ding and Farmer at almost the same wind speed, but the distribution of event speeds was narrower—the fastest breaking wave events observed had line-of-sight speeds of about 0.6 of the dominant wave speed. The measured histograms of number of events versus event speed  $c$  suggested that the smaller events with  $c < 3 \text{ m s}^{-1}$  were only incompletely counted so that the characteristics of only the faster events ( $3\text{--}6 \text{ m s}^{-1}$ ) were analyzed in detail. With the use of independent data on the average shape of broken areas, for the first time the form of the function  $\Lambda(c)$ , the distribution with respect to speed of the length of breaking front per unit area of surface and  $c\Lambda(c)$ , and the fraction of surface turned over per unit time per speed increment were determined. These were found to decrease monotonically with increasing event speed, indicating that these quantities are dominated by the smaller, more frequent breaking events. By making use of the Duncan–Melville expression for the dissipation rate per unit length of a breaking front, the distributions of wave energy dissipation by breaking and of momentum flux to the water by breaking wave impulses are also found for the first time. These were found to be broadband over the whole range of breaker speeds that could be measured reliably, that is, those corresponding to scales of 50%–20% of the dominant wavelength. These results offer no support to the hypothesis of a “Kolmogorov cascade” in wind-generated waves analogous to that in turbulence, with energy input from the wind at large scales and dissipation from the waves at small scales. The measurements indicate that, in contrast, dissipation is significant at the largest scales of wave breaking and is distributed widely across that spectrum. If the results are interpreted in terms of equilibrium range wave theory, a value for the numerical constant in the Duncan–Melville expression is inferred that is smaller than the range given by Melville, but a simple expression for the total rate of energy loss from the wind-driven waves is quantitatively consistent with results of upper-ocean turbulence dissipation measurements reported by Terray et al.

### 1. Introduction

Wave breaking in a wind-generated sea is one of the most important but least understood statistical and dynamical processes that occur in the upper ocean. The phenomenon is sporadic and fugitive; individual events appear almost randomly in space and time, ride along with a wave crest for a brief time, and then subside. Breaking occurs over a very wide range of scales. At

one end there may be waves possibly hundreds of meters long with crests moving almost as fast as the wind, and at the other we see short gravity waves 10 or 15 cm long that support microscale breaking with turbulence but almost no air entrainment. Wave breaking is transient but locally violent. It is generally agreed that it provides the dominant mechanism for the dissipation of the energy of gravity waves and the generation of near-surface turbulence. Breaking events provide local impulses, transferring momentum from the propagating waves to the near-surface water, but the role of this in the overall air–sea momentum transfer has only recently been quantified by Banner and Peirson (1998). In the absence of wave breaking, interfacial gas transfer is

---

*Corresponding author address:* Dr. Owen Phillips, Dept. of Earth and Planetary Sciences, The Johns Hopkins University, Baltimore, MD 21218-2687.  
E-mail: omphil@aol.com

impeded by the diffusive surface layer, but breaking disrupts this barrier by turning the surface under, injecting bubbles into the water and drops into the air.

Very little information is available on the statistical dynamics of breaking wind-generated waves, but there are various speculations. Numerical wave models developed during the last 30 years (SWAMP Group 1985; Komen et al. 1994) have been based on the transport or spectral balance equation expressing the rate of change of energy or action spectral density, moving with the wave group velocity, in terms of three dynamical processes—energy input from the wind, wave–wave interactions, and dissipation by wave breaking. The first two are distinct dynamical processes that have attracted considerable theoretical, experimental, and observational attention; though problems remain, they are in principle calculable. Dissipation has remained a problem. As part of his pioneering development of numerical wave modeling following JONSWAP, Hasselmann (1974) proposed a dissipation source function that incorporated only general physical constraints together with considerable empiricism that has been modified (tuned) over the years to allow the model to reproduce observed wave spectral shapes and growth rates. It is still used extensively. A quite different approach has been taken by Kitaigorodskii (1983, 1992), Zakharoff (1992), Zakharoff and Zaslavskii (1982, 1983), and others. In their “weak turbulence theory of wind waves,” it is assumed (in an analogy with the Kolmogorov theory of turbulence) that energy input from the wind occurs predominantly to the largest waves and that dissipation is concentrated at the smallest scales (Kitaigorodskii 1992b). It is postulated that wave–wave interactions provide an almost constant spectral flux through the intervening wave scales. There is no direct evidence for the validity of this description (and simple visual observation of breaking waves seems to contradict it), but the theoretical development based on it is purely deductive and quite elegant and has predicted spectral shapes quite close to some of those observed. However, it appears that the spectral shapes over frequencies and wavenumbers that are large compared with those of the spectral peak are poor tests for theory—even with different physical assumptions, the spectral slopes predicted vary by only about 10% among simulations. In contrast to the weak turbulence theory, the equilibrium range theory for wind-generated gravity waves (Phillips 1985) assumes that in a developed sea, all three processes are comparable in this range. The wind input is determined by the characteristics of the airflow over the moving waves, and the wave–wave interactions resulting from the nonlinearity of the free surface water motion develop as the wave components grow. Surface current convergence or divergence can increase or decrease the energy (though not action) spectral density. As mentioned earlier, in principle these processes can be calculated separately. In contrast, wave breaking occurs following local instabilities that become more fre-

quent as the waves become more energetic. Under steady wind conditions, a quasi-equilibrium develops at high wavenumbers and frequencies and the net energy supplied by the other processes determines the number density and distribution characteristics of the breaking events required to provide the dissipation.

Quantitative measurement of wave breaking at sea is extremely difficult and the only feasible techniques involve remote sensing. Measurements of whitecap coverage by analysis of photographs have of course been made for a number of years, notably by Monahan (1971) and Monahan and O’Muircheartaigh (1980). The results are difficult to interpret in dynamical terms and show a great deal of scatter, as Wu (1980) and others have noted. A most notable pioneering study by Ding and Farmer (1994) located by acoustic triangulation the near-surface underwater sound sources produced by breaking and recorded their inception, propagation, and demise. In this paper, we report on measurements also on individual breaking events in a wind-generated sea, but taken with a high range resolution microwave radar operating at very low grazing angles. Ding and Farmer’s measurements were obtained over a much wider range of conditions than were the radar data available to us, but the radar data have much higher resolution—intercomparison of the two sets is revealing. The radar measurements were made under Office of Naval Research sponsorship by Hansen and other members of the Naval Research Laboratory Radar Division in 1994, the data were described, edited, and prepared for analysis by Posner (1998b) and the oceanographic analyses were made by Phillips.

## 2. The measurements

Between August and December of 1994, the U.S. Naval Research Laboratory (NRL) conducted an extensive series of X-band (9.5–10.0 GHz) radar measurements of sea clutter at low grazing angles from sites in Kauai, Hawaii. The very short transmitted pulses yielded data from a range of 3.5 n mi (6.5 km) over a swath with a range resolution of 1 foot (30.5 cm) and range extent of 512 feet (156 m) in the data used here; the beamwidth was  $2.4^\circ$  in azimuth, or about 270 m at the range of 6.5 km. The pulse repetition frequency was 2000 Hz. Measurements were made with the radar directed upwind and crosswind in both horizontal transmit-and-receive (hh) and vertical transmit-and-receive (vv) modes. A detailed account of the specifications of the equipment and data acquisition is given in an NRL Report by Posner (1998). In essence, the ribbon-shaped footprint, 30 cm in range and 270 m in azimuth, sweeps in range down the swath, and a return is generated by any target in the short range interval, whatever its azimuth position. The repeated scans enable the precise tracking of a transient target in range (though not to any significant extent in azimuth) from its inception until it

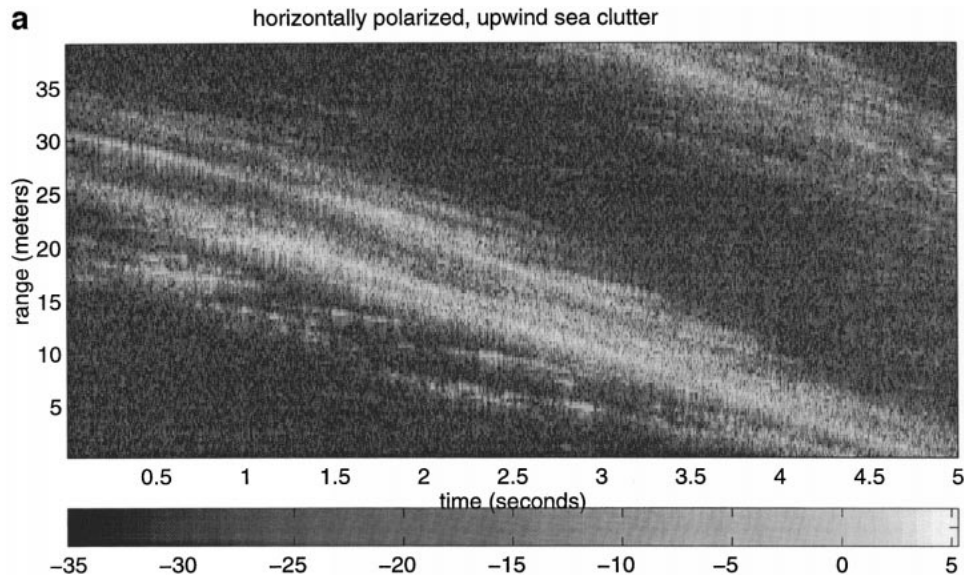


FIG. 1a. A range-time plot of the radar cross section of a small section of the upwind-hh (horizontally polarized transmission and reception) data, taken at a very low grazing angle. The ribbon-shaped footprint, 30 cm in range and 270 m in azimuth sweeps down range at a frequency of 2000 Hz. Individual traces are produced by transient breaking events moving toward the radar at speeds given by their slopes. Overlapping traces are indicative of the simultaneous occurrence of multiple events in the footprint at different locations in the 270-m azimuth. Detailed information and further examples are given by Posner (1998b).

disappears so that its duration and speed in the range direction can be found.

The data that we examine were obtained on 8 November 1994 from a radar system at the top of a cliff on the coastline adjacent to Lihue airport, Hawaii. The fetch was in effect infinite. Directional wave spectra

were measured during the wave observation period and J. Hanson of the Johns Hopkins Applied Physics Laboratory has very kindly made them available to us. The directional distribution of the energy-containing components was very narrow, concentrated within  $\pm 30^\circ$  of the dominant wave direction, coming from  $80^\circ$ . The

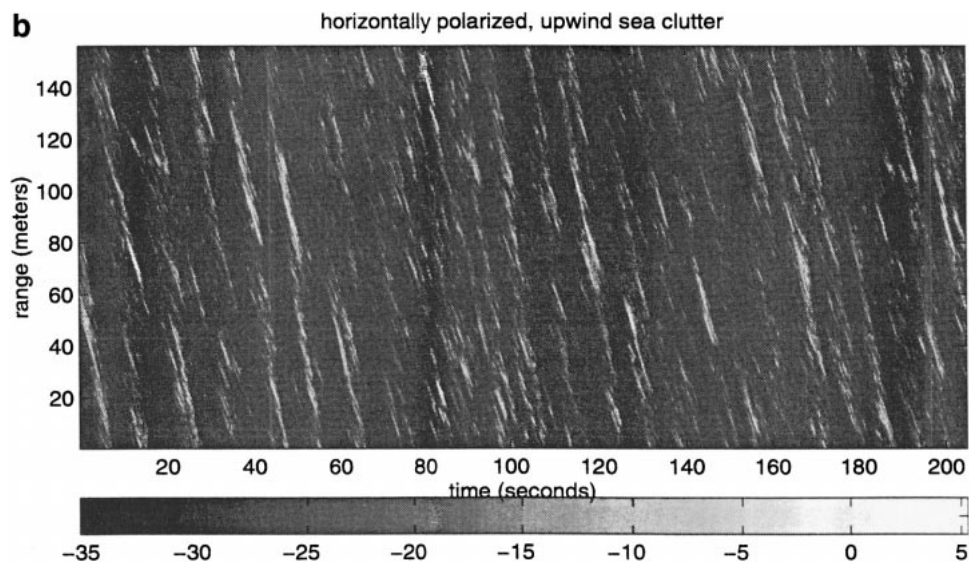


FIG. 1b. Upwind-hh backscattered data over the full range swath of 156 m for a time interval of about 200 s. The modulations, bands of high return that are most evident in the first 60 seconds of the record are the result of a rather groupy 9.7-s swell moving toward the radar. This is also detected by the directional wave buoy. Upwind vv data are similar, but somewhat more diffuse. The gray scales are dB relative to  $1 \text{ m}^2$ .

overall significant wave height, measured by a directional wave buoy, was  $(3.0 \pm 0.1)$  m, with the dominant 7.1-s wind wave having a calculated phase speed of  $11.1 \text{ m s}^{-1}$ , and a 9.7-s swell also from  $80^\circ$  having wavelength 147 m and phase speed  $15.15 \text{ m s}^{-1}$ . During the early afternoon when the vv measurements were made, the wind speed was steady in magnitude ( $9.3 \pm 0.3 \text{ m s}^{-1}$ ) and direction ( $73^\circ$ , trending toward  $80^\circ$ ), and it was essentially the same 18 hours later. During the late afternoon when the hh measurements were made, the wind speed was unfortunately not being measured, but the steadiness during the preceding and following time periods and the consistency that we will find between the hh and vv measurements, leads us to believe that the wind was essentially steady throughout.

A small sample of the data from a range interval of 30.5 m over 5 seconds is shown in Fig. 1a. In this instance, the radar was directed upwind ( $78^\circ$ ) and horizontally polarized in both transmission and reception (hh). The display, which can be interpreted as an  $x-t$  diagram, shows signals from a number of events, breaking fronts we believe, at ranges that decrease with time, approaching the radar at speeds proportional to the slopes of the traces on the display. Some begin and end fairly clearly within the domain, though the onset and disappearance times may be uncertain to about 0.2 s. In the region of most intense return in this sample, individual events are more difficult to identify. A breaking front whose normal is inclined to the direction of looking produces signal in several adjacent range bins in any one scan, and so smears the pattern in the vertical. A faster breaking front overtaking a slower one produces two convergent traces that merge when their ranges coincide, even though the waves may be at opposite ends of the footprint and displaced from each other in the azimuthal direction by as much as 270 m. Some traces below the region of brightest return exemplify this. When the traces merge completely, as in parts of that region, it may not be possible to pick out individual events in the tangle, so there is an inevitable undercounting. In about 30% of the detectable events in the data, one end of the track was clear, but the other end was obscured, as can be seen in parts of Fig. 1a. Since it is unlikely that the separate events were interacting dynamically because of the large extent of the footprint in azimuth, it was assumed that the partially obscured events have the same statistics as those that occur singly. Tangling and overlapping images could be reduced by reduction of the azimuthal beamwidth, but this experiment was performed for another purpose, and its application to breaking wave dynamics has been serendipitous. The undercounting, as we will see from the results, is most serious for the shorter, slower (and by inference, smaller) events and places a lower limit to the ranges over which the results can be considered useful.

Fig. 1b is a similar range/time plot of radar cross section for a more extensive set of about 200 seconds

of hh-upwind data. The influence of the 9.7 s swell detected by the directional wave buoy is evident in the large-scale modulations whose slope is consistent with the phase speed calculated from the dispersion relation. The modulations could have been produced by either or both of two separate effects. Short waves riding on swell are amplified near the swell crests and so are more likely to break there than in the trough region where their amplitudes are lowest. In addition, the troughs were to some extent in the "radar shadow" of the preceding swell crest and a breaking wavelet there is less likely to return a measurable signal. These swell modulations could result in undercounting the breaking events by a factor of about 2, but this is a good bit less than the present order-of-magnitude uncertainties in many wave breaking statistics. More significantly, the concentration of breaking events near the swell crests produces a bias in the measurement of event speed because of the forward advection there; this is considered later.

A number of characteristics of the return signals are consistent with an identification of the targets as the tumbling fronts of breaking waves as Wetzel (1986) suggested. The spatial distribution patterns, lifetimes, and speeds of propagation are generally consistent with this identification. Particularly persuasive are short-interval (2–5 millisecond) variations of radar cross section from a particular range cell, such as shown in Fig. 2. The return signal was clearly unsteady and presumably the target was also; relative movement of different elements of the target would produce variations in the phases of the returns from separate elements and interference with high-frequency variations in the net return. The depth of the high-frequency modulations is surprisingly large. The wavelength of the radar is about 3 cm, so variations in signal strength in 2 ms by phase interference would be produced by relative motions between elements of the target of about  $7.5 \text{ m s}^{-1}$ . This, as will be seen, is of the same order of magnitude as the water velocities expected in the breaking regions during the conditions of observation.

The upwind/hh images were the sharpest, spikiest, and most intermittent, and therefore the easiest to analyze. The upwind/vv images were rather more diffuse, which made the identification of individual events more questionable in some cases. The crosswind/hh and vv images were broader and the return signals generally smaller by about 10 dB. As pointed out by Posner (1998) there may have been some problem with the orientations of the nominally crosswind observations, so we will not consider them further here.

### 3. Kinematical analyses

Because of the lack of azimuthal resolution, there were no observations of the directionality of breaking events. The directional distribution of the dominant components of the wave field was quite narrow, as doc-

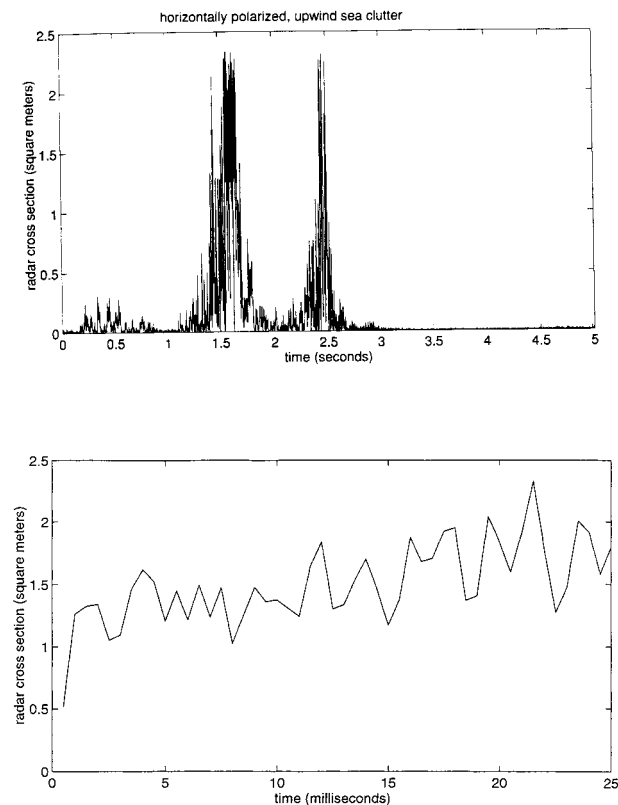


FIG. 2. Short histories at different timescales of the upwind-hh backscatter from a single range cell as breaking events pass through it. Note the magnitude of the returns (radar cross sections of order  $1 \text{ m}^2$ ) and the very deep modulations on timescales 2–10 ms.

umented previously, with wind, swell, and dominant waves closely aligned. Under these seemingly ideal conditions, one would expect that the directionality of the motion of larger-scale breaking fronts would also be narrow. Note, however, that Ding and Farmer's directional distributions at  $10 \text{ m s}^{-1}$  show a very wide spread—38% of the observations are beyond  $\pm 45^\circ$  of the wind direction and 13% of the total number were apparently moving against the wind. No such events were recorded by the radar. In the analyses that follow, it will be supposed that in these observations, the directional distribution of breaking was narrow and that all breaking fronts measured were indeed traveling close to the wind direction. The kinematical and dynamical distributions that will be inferred below involve the breaking front speeds raised to positive powers, so that contributions from events moving at substantial angles to the wind will be underestimated.

On the other hand, the front speeds measured are relative to the fixed radar, and include the advective effects of the swell. Quantities such as the rate of energy dissipation depend on the intrinsic speed of the breaking front, that is, the speed relative to the underlying water. Because of the modulations in the density of breaking events observed, with maxima apparently near the swell

crests, a systematic bias upward is introduced into the speed measurements. From the directional wave spectra, the significant wave height of the swell was estimated to be approximately 2.1 m and with use of the measured swell wavelength of 1.50 m, the swell slope  $ak$  is found to be 0.042 and the fluid velocity at the swell crest is found to be  $0.7 \text{ m s}^{-1}$ . Most of the measurable events in the data occurred within  $60^\circ$  of the crest, and the average advection velocity over this interval is found to be approximately  $0.35 \text{ m s}^{-1}$  toward the radar. This probably overestimates the correction somewhat since the swell-induced modulations shown in Fig. 1 appear to be somewhat groupy. Nevertheless, the intrinsic speed will then be taken as the measured speed less this swell advection speed, so best estimates may be intermediate between uncorrected and “corrected” values. Ding and Farmer (1994) in a footnote find this correction to be insignificant in their measurements, but when we estimate the distributions of momentum and energy fluxes that involve the speed to the fourth and fifth powers, it can be significant. Because of the somewhat ad hoc nature of this correction, results will be shown both with and without it.

Another consequence of the lack of azimuthal resolution is the absence of information on the lengths of the breaking fronts in contrast to the distances that they move. Data obtained photographically by Bortkovskii (1987) show positive but scattered correlation between the downwind and crosswind dimensions of broken regions, with the mean length of breaking front being about twice the distance traveled. On the other hand, extensive sonar measurements by Thorpe (1982, 1986) and Thorpe and Hall (1983) found that the ratio of the mean length of breaking front to distance traveled was only about 0.7. In Snyder et al.'s (1983) observations, the breaking zones were also found to be elongated in the direction of advance. It is likely that, in nature, the ratio will depend on the wave directional distribution among other factors; since Thorpe's measurements were at long fetches and wind speeds that bracketed our conditions, we adopt the ratio  $r = 0.7$ .

The upwind/hh dataset was obtained from a swath area  $A$  of  $3.8 \times 10^4 \text{ m}^2$  over a time interval of 174.8 seconds, during which 733 breaking events were detected, 519 of which were measurable in the sense that their onset and disappearance times and ranges could be determined. The event density, the number of events per unit area per unit time, was  $1.2 \times 10^{-4} \text{ m}^{-2} \text{ s}^{-1}$ , compared with a value of  $2.5 \times 10^{-4} \text{ m}^{-2} \text{ s}^{-1}$  measured by Ding and Farmer at the same wind speed. The upwind hh data were divided into two segments, A and B of 76.8 and 98 seconds respectively, which were analyzed separately as a check on consistency. An additional 98 s of upwind/vv data with 306 measurable breaking events were also analyzed, and the results from the vv and hh data will be seen to mix quite well. Histograms with respect to event speed duration are shown in Fig. 3, together with similar results of Ding and Farmer at

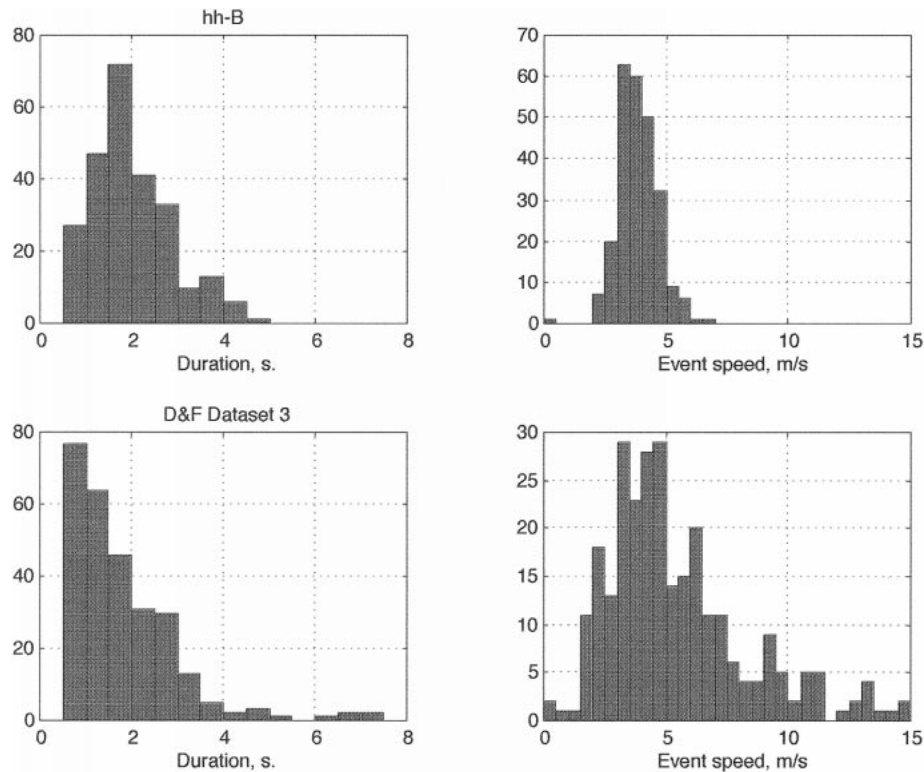


FIG. 3. Histograms of breaking event durations (left panels) and event speeds (right panels) is from our radar measurements (set hh-B) and the bottom row is of measurements of Ding and Farmer (1994), dataset 3. In the radar observations, the wind speed was  $9.3 \text{ m s}^{-1}$  and the dominant wave speed was  $11.1 \text{ m s}^{-1}$ , while the acoustic measurements were at a wind speed of  $10 \text{ m s}^{-1}$  and a dominant wave speed of  $12 \text{ m s}^{-1}$ .

about the same wind speed. It is immediately apparent that the distributions measured acoustically are significantly broader than those measured by the radar. The fastest breaking waves that we observed had speeds of about 0.6 of the dominant wave speed ( $11.1 \text{ m s}^{-1}$ ), while Ding and Farmer found a number of events moving substantially faster than the dominant waves, and indeed, some faster than the wind. The range resolution of the radar is very much higher than is possible to obtain acoustically, but the differences are more than we would have expected.

In our measurements, the number of occurrences increases monotonically as the event speed decreases until  $c \approx 3 \text{ m s}^{-1}$ ,  $c/c_p \approx 0.4$ , after which it appears to drop abruptly. It is hardly credible that the actual frequency of occurrence of slower moving, smaller, and usually briefer breakers is less than that of faster, larger ones. Visual observation suggests that the number densities should continue to increase with decreasing scale, though the smaller, slower events entrain less air and produce less foam. They have more the nature of a short duration splashing or microscale breaking with almost no air entrainment. Evidently, the absence of observations at small scales is a result not of the absence of breakers at these scales, but of the lack of our ability

to measure or detect them. The acoustic signals are produced by entrained bubbles, and their presence is required for detection. The smaller events have smaller radar cross sections and generally had shorter durations and when the duration of a breaker was less than about 1 s, it was very difficult to estimate its speed from the trace. Accordingly, many of these had to be ignored. *We therefore discount as not credible any measurements involving the number densities of waves for which  $c < 3 \text{ m s}^{-1}$ .* The speed and duration distributions given by Ding and Farmer, shown in Fig. 3 for a wind speed of  $10 \text{ m s}^{-1}$ , have their maxima at rather lower values than ours and extend down to speeds of  $1.8 \text{ m s}^{-1}$  and durations of 0.5 s. Apparently, Ding and Farmer's acoustic technique was able to measure more of the shorter, slower events than we could from the radar traces, which may account for the larger event density they observe.

Figure 4 shows the mean event duration measured plotted against the mean apparent speed (i.e., without the crest advection correction) of breaking events in each bin. Measurements from the two segments of hh-upwind and one of vv-upwind data are identified separately, and the three sets do mingle reasonably well. The difficulty of measuring short-duration, low-speed events suggests that the mean durations of measured

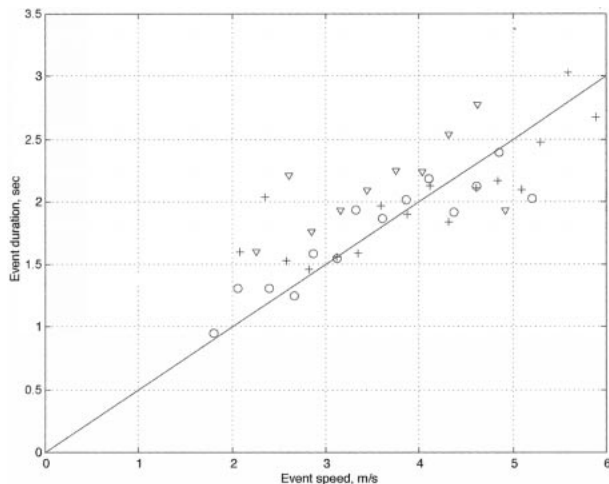


FIG. 4. Mean durations of breaking events grouped in speed bins of width  $0.25 \text{ m s}^{-1}$ . Data points are:  $\circ$  = hh A;  $+$  = hh B;  $\nabla$  = vv.

events with speeds below about  $3 \text{ m s}^{-1}$  are likely to be biased high. With this proviso, the results show a fairly clear linear proportionality between the mean duration  $\tau$  and the event speed, consistent with the relation  $\tau = 5(c/g) \cong 0.8$  times the wave period. If we define a “wavelength” of the breaker as  $\lambda_b = 2\pi c^2/g$ , then the mean length of the breaking zone  $\tau c \approx (5/2\pi)\lambda_b \approx 0.8\lambda_b$ . Rapp and Melville (1990) found that this expression summarized their laboratory measurements also, though Thorpe (1986, Fig. 13) shows a quite strong dependence of the coefficient 0.8, above, on  $U/c$ . Ding and Farmer (1994) found no consistent relationship between duration of breaking and event speed.

#### 4. Dynamical properties

##### a. $\Lambda(c)$ : The average length of breaking front per unit area per unit speed interval

A single breaking event is generally initiated at some point on the wave crest and spreads laterally so that its average length is of order half its ultimate length, the width of the broken patch. If it moves in the wind direction with speed  $c$  and duration  $\tau$ , then according to Thorpe’s result, its expected ultimate length is about  $0.7 c\tau$  so that its *average* length over the duration of the event is about  $0.35c\tau = \alpha c\tau$ , say. This individual event lasts for the fraction  $(\tau/T)$  of the total observation time  $T$  so that, at an arbitrary instant during the observation interval, the expected length to be observed is  $\alpha c\tau(\tau/T)$ . If we consider all events in the speed range  $c, c + \Delta c$ , then the expected total length of breaking fronts at any instant of the observation time period is  $\alpha \sum c\tau(\tau/T)$ , where the summation is over all events in that speed interval. If  $A$  represents the swath area, the area of the sea surface under observation, then the average length of breaking front per unit area per unit speed interval is given by

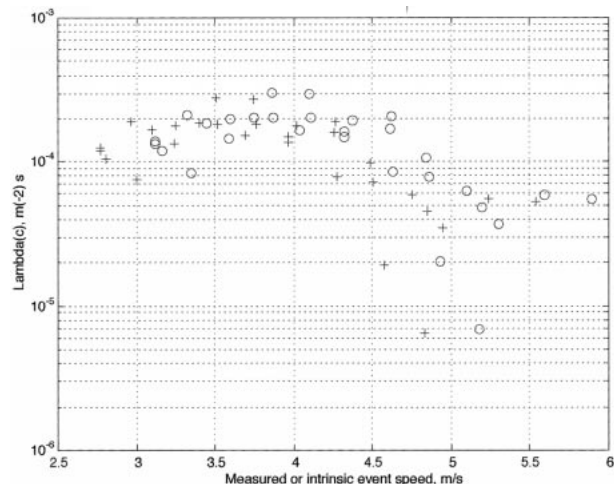


FIG. 5. Measurements of  $\Lambda(c)$ , the average length of breaking front per unit area per unit speed interval, with (+) and without ( $\circ$ ) correction for swell advection. Points for velocities less than about  $3\text{--}3.5 \text{ m s}^{-1}$  are not believed to be reliable; the scatter at the largest speeds is a consequence of the small number of these events in the samples.

$$\Lambda(c) \approx \alpha c \left( \sum \tau^2 \right) / (AT\Delta c). \quad (1)$$

This function is of key importance in the statistical mechanics of breaking waves, in questions concerning (i) the rate at which surface water is turned under in wind-generated waves, (ii) the generation of turbulence in the upper mixed layer, (iii) the momentum flux from waves to the upper mixed layer by the impulses of breaking events, and (iv) the rate of exchange of gases across the air–sea interface. It has not been measured hitherto, but a first estimate can be made from the observations reported here. As mentioned earlier, they were obtained for another purpose, and not optimized for the measurement of individual wave events. For this application, the limitations of these data are substantial, particularly the relatively small sample sizes, the difficulty of identifying small events, the less-than-optimal azimuthal width of the swath with a substantial fraction of overlapping traces, and the lack of data at different wind speeds. Judging from the scatter of the measurements and possible uncertainties about systematic errors, one could hardly claim accuracy in the results below of better than a factor of about 3. Nevertheless, the results do answer some questions and raise others.

Figure 5 shows  $\Lambda(c)$  calculated from the measured statistics of the breaking events with use of Eq. (1). It is not useful to identify the different data segments separately, but they are shown uncorrected (circles) and corrected (crosses). Events with apparent line-of-sight speeds of advance less than  $3 \text{ m s}^{-1}$  were in essence ignored. In this plot, the advection correction is seen to shift the points to the left and reduce the ordinate slightly, but the effect of the latter is small compared with the scatter in the data. The apparent maximum near  $3.5\text{--}4 \text{ m s}^{-1}$  is probably not real, but an indication of a

proportion of missed smaller and slower events. This figure demonstrates that the faster, generally larger breaking events make smaller contributions to the total length of breaking front than do slower, generally smaller events because of the increased frequency of the latter. This is certainly consistent with casual observation of the sea surface on a windy day. The first moment,  $c\Lambda(c)$ , represents the distribution with respect to breaker speed of the rate at which the fronts sweep out area, that is, of the rate of surface turnover, the fraction turned under per second per speed interval, a quantity that is important in questions of gas exchange. Since we can consider the whole area as an ensemble of individual points, the quantity  $c\Lambda(c)dc$  can also be interpreted as the number of breaking waves in the speed interval  $dc$  passing a given point per unit time. This function is not shown separately. The total turnover rate is also dominated by the smaller events, though the slope of the function at high event speeds is of course a little less than in Fig. 5 and its magnitude (in  $m^{-1}$ ) is three to six times larger.

*b. Distribution of wave energy dissipation by breaking*

Of greater dynamical interest is the distribution of wave energy loss by wave breaking. Duncan (1981) generated statistically steady, turbulent deep water breakers in a laboratory tank and showed that the rate of energy loss per unit length of breaking front is proportional to  $\rho_w g^{-1} c^5$ , where  $\rho_w$  is the water density, with a constant of proportionality that is numerically small. This smallness can be anticipated from a very simple model. At breaking, a jet of water with speed of about  $c$  is ejected forward with energy flux per unit length of front  $\frac{1}{2}\rho_w c^2 c\delta$ , where  $\delta$  represents the vertical thickness of the jet. This is a *very* small fraction of the wavelength of the breaking wave, namely,  $2\pi c^2/g$ , so that the energy flux per unit width from the wave is an equally small fraction of  $\pi\rho_w c^5/g$ . In quasi-steady breaking waves, Duncan's laboratory measurements indicate a value of the proportionality coefficient  $b$  of about 0.03, but one would expect that the numerical coefficient would be smaller in the transient events characteristic of open sea, moderate weather events. In a careful review, Melville (1994) showed that this is indeed so, and inferred that in transient breakers  $b \approx (3 \text{ to } 16) \times 10^{-3}$ . Because of the present uncertainty in this quantity, we calculate

$$\varepsilon(c)/b = \alpha\rho_w g^{-1} c^5 \Lambda(c), \quad (2)$$

making use of the data of Fig. 5. The result is shown in Fig. 6. Again, the uncorrected points are shown as circles, the corrected as crosses.

It is immediately evident that the distribution is broadbanded over the range of event speeds above about  $3 \text{ m s}^{-1}$ . The drop-off below about  $3.5 \text{ m s}^{-1}$  is probably indicative of the existence of some unmeasured events and the scatter at speeds above  $4.5\text{--}5 \text{ m s}^{-1}$  reflects the small number of large, rapidly moving breaking events

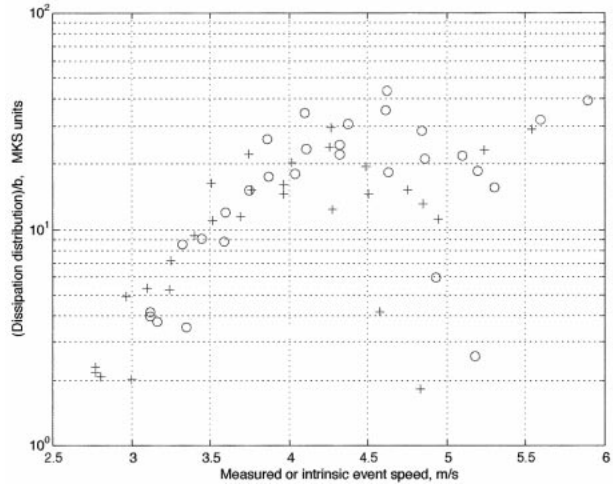


FIG. 6. The distribution of wave energy dissipation by breaking with respect to event speed, divided by the numerical factor  $b$  in Duncan's energy loss expression. Symbols for the points are as in Fig. 4.

in the sample sizes. In the midrange, however, the measurements from different data segments define the level of the dissipation distribution well, with most corrected points lying in the range  $15 < \varepsilon(c)/b < 30$  in MKS units ( $\text{kg m}^{-1} \text{s}^{-2}$ ) and uncorrected between 20 and 40. The overall effect of the corrections is small compared with the scatter. Over the short range of event speeds, there is no obvious trend in the level of the dissipation rate per unit area per unit speed interval.

The range of breaker speeds covered by these measurements is certainly small, but the results of Fig. 6 give no support to the basic assumption of the weak turbulence theory of wind waves that the energy dissipation from waves is concentrated at the smallest scales. It appears to be distributed broadly over the range for which our measurements seem to be reliable.

*c. Distribution of momentum loss rate in breaking wave impulses*

Since wave energy and momentum densities are related as  $M = E/c$ , the loss of wave energy in breaking is accompanied by an impulse on the water surface and an overall downward momentum flux from the wave field, which, in a quasi-equilibrium state, cannot exceed the overall wind stress, but may be a substantial part of it (Banner and Peirson 1998). The distribution  $I(c)$  of this momentum flux with respect to wave speed is, from Eq. (2),

$$I(c)/b = \alpha\rho_w g^{-1} c^4 \Lambda(c), \quad (3)$$

which is shown in Fig. 7. Again, the points near the ends of the speed range are probably less significant and, if less weight is given to points representing speeds less than  $3\text{--}3.5 \text{ m s}^{-1}$ , there is again little obvious trend. In the midrange, between  $3.5$  and  $5 \text{ m s}^{-1}$ , the corrected

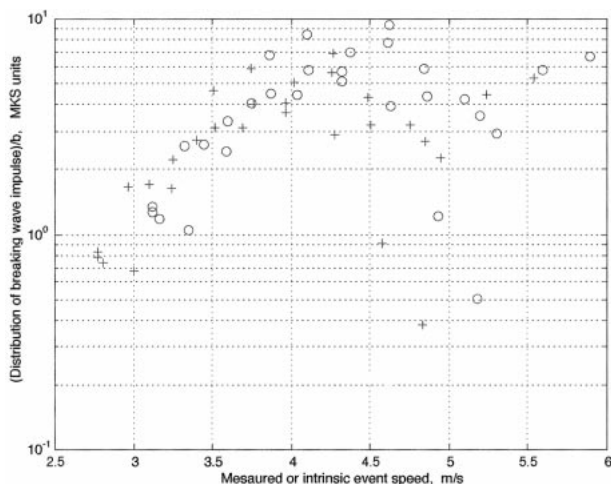


FIG. 7. The distribution of breaking wave impulse, or momentum flux, with respect to event speed, again divided by  $b$ . Symbols as in Fig. 4.

points mostly lie in the range  $3 < I(c)/b < 6$  in MKS units of density  $\times$  velocity. Uncorrected points are mostly between 4 and 8.

## 5. Integrated fluxes

In the measurements described above, the levels in the distributions are defined reasonably well, but only over a narrow range. The algebraic forms of the distributions are given by equilibrium range theory with numerical coefficients that are known only poorly, and they have not yet been tested by observation. These results cover too small a range of breaking front speeds to define the power laws involved, but if one tentatively accepts these equilibrium range expressions, the measurements can be used to calibrate them and to interrelate these measurements with independent results on upper-ocean momentum flux and wave energy dissipation by breaking.

According to this theory (Phillips 1985, 524–526), the one-dimensional distribution with respect to event speed of the impulse provided by wave breaking (the wave breaking momentum flux) is given by

$$I(c) = E\rho_a u_*^3 c^{-2}, \quad (4)$$

where  $E$  is a numerical factor known a priori to be of order unity,  $u_*$  is the friction velocity, and  $\rho_a \approx 1.3 \text{ kg m}^{-3}$  is the air density. The total wave breaking momentum flux,  $\tau_w$ , which in an equilibrium state is equal to the momentum flux from wind to the waves in the equilibrium range, is the integral of (4) from the speed of the fastest breaking waves (about  $0.6U_{10}$ ) to that of the shortest. The surface drift velocity, proportional to and somewhat smaller than  $u_*$ , provides a lower limit to the speed of short breaking gravity waves (microscale breakers), as Banner and Pierson (1998) indicate in their

careful study of the air–sea momentum flux processes. Thus

$$\tau_w = E\rho_a u_*^2 \{1 - O(u_*/U_{10})\}. \quad (5)$$

The second term in the parentheses is about 0.04–0.05. Banner and Pierson also estimate that in a well-developed wave field such as existed during these observations, approximately 70% of the total drag is supported by the waves so that in the expression (4) for the distribution of wave breaking momentum flux,  $E \approx 0.7$ . If Fig. 7 is taken to define the level of this distribution near  $c \approx 4.5 \text{ m s}^{-1}$ , we obtain an independent estimate for the open-sea value of the constant  $b$  in Duncan’s dissipation formula. Problems with the lack of simultaneous wind speed measurements have been described previously, but we take  $u_* \approx 0.45 \text{ m s}^{-1}$ . In the mid-range of Fig. 7,  $u_*/c \approx 0.1$  so that from the expression (4), when  $c \approx 4.5 \text{ m s}^{-1}$ ,  $I(c) \approx 4 \times 10^{-3} \text{ kg m}^{-2} \text{ s}^{-1}$ . But from Fig. 7,  $I(c)/b = 3$  to 6 in this range so that the factor  $b \approx (7 \text{ to } 13) \times 10^{-4}$ . This is smaller by a factor of about 5 than the range inferred by Melville (1994) from quite different data. The reasons for this discrepancy are not altogether clear, though it is gratifying that completely different approaches can give results that are within an order of magnitude of each other. It is hoped that more precise results will emerge in the future.

Equilibrium range theory also predicts that the distribution of wave energy dissipation with respect to (scalar) wave speed is

$$\varepsilon(c) = \hat{E}\rho_a u_*^3 c^{-1}, \quad (6)$$

[Phillips 1985, Eq. (6.6)], where the numerical constant  $\hat{E}$  is somewhat larger than  $E$  in (4) because, in (4), only the component of impulse in the wind direction contributes to the net momentum flux, whereas the energy losses simply add as scalars. The results of Fig. 6 are clearly inadequate to indicate any  $c^{-1}$  dependence but, if Eq. (6) is valid over a range of phase speeds with end points proportional to  $c_p$  and  $u_*$ , then the total wave dissipation is given by

$$\frac{\bar{\varepsilon}}{u_*} \approx \hat{E} \ln \left( G \frac{c_p}{u_*} \right), \quad (7)$$

where  $\bar{\varepsilon} = \varepsilon_0/(\rho_a u_*^2)$  is the very physically appealing quantity defined by Gemmrich et al. (1994) and is called the “effective phase speed” related to wind input. Here  $G$  is another numerical quantity of order unity. This is compared in Fig. 8 with measurements reported by Terray et al. (1996) of the total dissipation in upper-ocean-layer turbulence generated very largely by breaking waves. Although there is considerable scatter in the (very difficult) measurements, the overall shape is summarized well by the expression (7) with  $\hat{E}$  taken as 2.5 and  $G$  as 0.5. Uncertainties in the actual values of the endpoints of integration may displace the curve vertically by a unit or two, but there do seem to be the

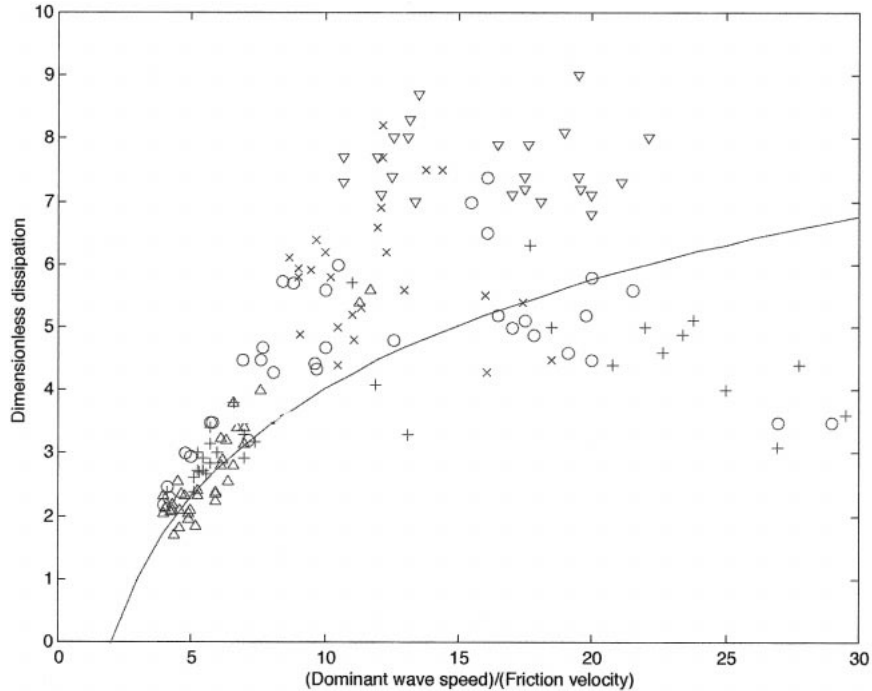


FIG. 8. Measurements reported by Terray et al. on the total energy dissipation rate  $\varepsilon$  in upper-ocean layer turbulence generated by breaking waves. The ordinate is  $\varepsilon/\rho_a u_*^3$ , where  $\rho_a$  is the air density and  $u_*$  the friction velocity. The ratio  $\varepsilon/\rho_a u_*^2$  is called by Gemmrich et al. (1994) the “effective phase speed” for energy flux from wind to waves. The triangles are from measurements by Kahma (1981) as cited by Terray et al. and are consistently higher than other points. The curve is the logarithmic formula (7) with  $\bar{E} = 2.5$  and  $G = 0.5$ , the form based on the radar measurements and equilibrium range theory.

beginnings of consistency among all these very different sets of measurements.

## 6. Some final comments

This high-resolution radar dataset provides a unique and potentially very valuable tool for air–sea interaction studies and, although we have extracted some useful results with it, the principal aim of this communication is to draw attention to its possibilities. We have been privileged to have had access to new and intriguing data that has already given new and valuable information, and has provided some lessons on the design of possible further measurements of this kind directed specifically to questions of air–sea interactions. The key ingredient is the high range resolution; the main omission is the lack of direct measurement of breaking front lengths and the principal problems with the data analysis were the proportion of overlapping traces and the swell-induced modulations. Are these the result of shadowing or of the well-known modulation of short waves by swell? These problems would be alleviated by observations at a shorter range and larger grazing angle, the first to reduce the azimuthal dimension of the footprint and the fraction of simultaneous events in a given range gate, and the second to reduce shadowing. Yet, to retain

the clarity of the identification of the radar returns as being from discrete breaking wave events requires that the grazing angle remain small, so a careful trade-off may be needed. Measurements such as these require the processing of huge amounts of data and have therefore been possible only recently. They also require the willing collaboration of people with quite different technical backgrounds, and this we have enjoyed.

*Acknowledgments.* We are very grateful to Dr. Merrill Skolnik, formerly Head of the Radar Division, Naval Research Laboratory, for his support and encouragement in the analysis of these data, and to Professors Stephen A. Thorpe and W. Ken Melville for their perceptive and very helpful comments; to Dr Jeffrey Hanson of the Johns Hopkins University Applied Physics Laboratory for his assistance in obtaining supplementary wind and wave data; and to Dr. Li Ding and Dr. David Farmer for allowing us access to their extensive acoustic datasets. We are grateful also to the anonymous referees for their careful reading of this manuscript. FP. was supported by the Office of Naval Research, Code ONR 31.

## REFERENCES

- Banner, M. L., and W. L. Peirson, 1998: Tangential stress beneath wind-driven air–water interfaces. *J. Fluid Mech.*, **364**, 115–146.

- Bortkovskii, R. S., 1987: *Air-Sea Exchange of Heat and Moisture during Storms*. D. Reidel, 194 pp.
- Ding, L., and D. M. Farmer, 1994: Observations of breaking surface wave statistics. *J. Phys. Oceanogr.*, **24**, 1368–1387.
- Duncan, J. H., 1981: An experimental investigation of breaking waves produced by a towed hydrofoil. *Proc. Roy. Soc. London*, **377A**, 331–348.
- Gemmrich, J. R., T. D. Mudge, and V. D. Polonchicko, 1994: On the energy input from wind to surface waves. *J. Phys. Oceanogr.*, **24**, 2413–2417.
- Hasselmann, K., 1974: On the spectral dissipation of ocean waves due to whitecapping. *Bound.-Layer Meteor.*, **6**, 107–127.
- Kahma, K. K., 1981: A study of the growth of the wave spectrum with fetch. *J. Phys. Oceanogr.*, **11**, 1503–1515.
- Kitaigorodskii, S. A., 1983: On the theory of the equilibrium range in the spectrum of wind-generated gravity waves. *J. Phys. Oceanogr.*, **13**, 816–827.
- , 1992: The dissipation subrange of wind-wave spectra. *Breaking Waves. Proc. IUTAM Symposium*, M. L. Banner and R. Grimshaw, Eds., Springer-Verlag, 200–206.
- Komen, G. J., L. Cavalieri, M. Donelan, K. Hasselmann, S. Hasselmann, and P. Janssen, 1994: *Dynamics and Modelling of Ocean Waves*. Cambridge University Press, 532 pp.
- Melville, W. K., 1994: Energy dissipation by breaking waves. *J. Phys. Oceanogr.*, **24**, 2041–2049.
- Monahan, E. C., 1971: Oceanic whitecaps. *J. Phys. Oceanogr.*, **1**, 139–144.
- , and I. O’Muircheartaigh, 1980: Optimal power-law description of oceanic whitecap coverage dependence on wind speed. *J. Phys. Oceanogr.*, **10**, 2094–2099.
- Phillips, O. M., 1985: Statistical and spectral properties of the equilibrium range in the spectrum of wind-generated gravity waves. *J. Fluid Mech.*, **156**, 505–531.
- Posner, F. L., 1998: Experimental observations at very low grazing angles of high range resolution microwave backscatter from the sea. U.S. Naval Research Laboratory Rep. NRL/MR/5310-98-8326, 53 pp.
- Rapp, R. J., and W. K. Melville, 1990: Laboratory measurements of deep-water breaking waves. *Philos. Trans. Roy. Soc. London*, **A331**, 735–800.
- Snyder, R. L., I. Smith, and R. M. Kennedy, 1983: On the formation of whitecaps by a threshold mechanism. Part III: Field experiments and comparison with theory. *J. Phys. Oceanogr.*, **13**, 1505–1518.
- SWAMP Group, 1985: *Ocean Wave Modeling*. Plenum Press, 2561 pp.
- Terray, E. A., M. A. Donelan, Y. C. Agrawal, W. M. Drennan, K. K. Kahma, A. J. Williams, P. A. Hwang, and S. A. Kitaigorodskii, 1996: Estimates of kinetic energy dissipation under breaking waves. *J. Phys. Oceanogr.*, **26**, 792–807.
- Thorpe, S. A., 1982: On the clouds of bubbles formed by breaking wind-waves in deep water and their role in air-sea gas transfer. *Philos. Trans. Roy. Soc. London*, **304A**, 155–210.
- , 1986: Measurements with an automatically recording inverted echo sounder, ARIES, and the bubble clouds. *J. Phys. Oceanogr.*, **16**, 1462–1478.
- , and A. J. Hall, 1983: The characteristics of breaking waves, bubble clouds and near-surface currents observed using sidescan sonar. *Contin. Shelf Res.*, **6**, 353–384.
- Wetzel, L., 1986: On microwave scattering by breaking waves. *Wave Dynamics and Radio Probing of the Ocean Surface*, O. M. Phillips and K. Hasselmann, Eds., Plenum Press, 273–284.
- Wu, J., 1988: Variations of whitecap coverage with wind stress and water temperature. *J. Phys. Oceanogr.*, **18**, 1448–1453.
- Zakharoff, V. E., 1992: Inverse and direct cascade in the wind-driven and surface wave turbulence and wave breaking. *Breaking Waves. Proc. IUTAM Symposium*, M. L. Banner and R. Grimshaw, Eds., Springer-Verlag, 70–91.
- , and M. M. Zaslavskii, 1982: The kinetic equation and Kolmogorov spectra in the weak turbulence theory of wind waves. *Izv. Atmos. Oceanic Phys.*, **18**, 747–753.
- , and —, 1983: Shape of the spectrum of energy-carrying components of a water surface in the weak-turbulence theory of wind waves (English translation). *Izv. Atmos. Oceanic Phys.*, **19** (3), 207–212.